Extremely large anisotropic transport caused by electronic phase separation in Ti-doped $Ca_3Ru_2O_7$

Extremely large anisotropic transport caused by electronic phase separation in Ti-doped $Ca_3Ru_2O_7$

Jin Peng[a, b], J. Y. Liu[b], Xiaomin Gu[a], Guotai Zhou[a], Wei Wang[a], J. Hu[b], F. M. Zhang[a] and X. S. Wu[a, *]

[a] *Collaborative Innovation Center of Advanced Microstructures, Lab of Solid State Microstructures, School of Physics, Nanjing University, Nanjing 210093, P. R. China*

[b] *Department of Physics and Engineering Physics, Tulane University, New Orleans, Louisiana 70118, USA*

Abstract

In this paper, we reported an extremely large out-of-plane/in-plane anisotropic transport (ρ_c/ρ_{ab}~ 10^9) in double layer ruthenates. The mechanism that may be responsible for this phenomenon is also explored here. Distinct from previously well studied layered materials which show large out-of-plane/in-plane electronic anisotropy (10^3 ~ 10^6), the Ti doped $Ca_3Ru_2O_7$ single crystals not only form quasi-2D layered structure, but also show phase separation within the layers. We found that Ti doping in $Ca_3Ru_2O_7$ induced electronic phase separation between the insulating phase and weak localized phase. The ratio of these two phases is very sensitive to the Ti concentration. At typical concentration, the weak localized phase may forms a channel on the background of insulating phase within the *ab* plane. However, the small volume of weak localized phase makes it less likely to overlap in different layers. This results in a much larger electronic anisotropy ratio than pristine compound $Ca_3Ru_2O_7$. This new mechanism provides a route for further increase electronic anisotropy, which will remarkably reduce current leak and power consumption in electronic devices.

Keywords: ruthenates, phase separation, electronic anisotropy.

* Corresponding author.
E-mail address: xswu@nju.edu.cn

1. Introduction

Transition metal oxides (TMOs) have been widely studied during last few decades since they have a wide range of unique behaviors owing to several simultaneously active degrees of freedom involving charge, spin, lattice and orbital.[1] The most famous compounds of this system are high-temperature superconductivity cuprates [2] and colossal magnetoresistivity manganites.[3] A productive area of TMOs is Ruddlesden-Popper (RP) type layered materials $A_{n+1}B_nO_{3n+1}$, where A can be trivalent rare-earth or divalent alkaline-earth ions; B is transition metal ions.[4,5] These types of materials are built by alternate stacking of *n*-layers BO_2 and rock-salt-type block layers A_2O_2 along *c*-axis. Therefore, even prepared as 3D bulk crystals, these materials can be viewed asquasi-2D layered structure. One of the most remarkable feature of these quasi-2D materials is their anisotropic characteristic, resulting in special properties in charge-transport, magnetic, optical conductivity, thermal conductivity and so on. These properties favor applications in industry, such as spintronic device,[6] magnetic sensor,[7] navigation systems, *et al*.

For anisotropic transport properties based applications, a large out-of-plane/in-plane transport anisotropy ratio (defined as ρ_c/ρ_{ab}) is one of the most important goals. In electrodes, sensors, transistors, it can remarkably reduce current leakage and power consumption.[8] In pixilated displays, it is strongly related to crosstalk.[9] Many kinds of layered materials (including bulk quasi-2D materials, films, organic-inorganic hybrid materials) have been synthesized and there anisotropic transport are extensively studied. In optimally doped single layered cuprates $Bi_2Sr_{2-x}La_xCuO_{6+\delta}$,[10] the anisotropy ratio (AR) can reach as high as 10^6 and in double layered manganites $La_{2-2x}Sr_{1+2x}Mn_2O_7$, around 10^3.[11] In organic-inorganic hybrids function materials, anisotropic ratio can reach around 10^5.[8,9,12,13] For these types of materials, the anisotropic resistivity can be attributed to the morphology: the alternation of highly conductive layer (BO_2 layer in TMOs and organic layers in hybrid materials) and lower conductive layer (rock-salt-type layers A_2O_2 in TMOs and inorganic layers in hybrid materials) in the through-plane direction. The schematic diagrams of these two types of materials are shown in Figure 1. Efforts, such as trying different types of conductive layer and insulating layer; different manufacturing methods have been made to increase AR.[8,12] Unfortunately, AR were limited to around $10^3 \sim 10^6$ for this morphology.[9,10] In this letter, a new route, increasing the complexity of the materials, has been

proposed to further increase AR. A material with real composition $Ca_3(Ru_{0.972}Ti_{0.028})_2O_7$ whose AR is around 10^9 at 5 K was observed

$Ca_3Ru_2O_7$ which is the pristine compound of this system, undergoes an antiferromagnetic (AFM) transition at 56 K from high temperature Paramagnetic (PM) phase to AFM-a (ferromagnetic(FM) bilayers coupled antiferromagnetically along *c* axis with spin along *a/-a* axis), followed by a metal-insulator transition (MIT) at 48 K[14]. For single crystals grown by floating zone method, its in-plane resistivity recovers to metallic behavior below 30 K, resulting a quasi-2D metallic ground state [15]. While Photoconductivity and Raman spectroscopy measurements reveals a charge gap opening associate with the MIT,[16,17] angle-resolved photoemission spectroscopy measurements (ARPES) proved the existence of small metallic pockets survived at non-nested Fermi surface.[18] The reentrance of metallic state below 30 K originates from these small metallic pockets. Our previous work found that a few percent of Ti doping on Ru site can tune the system from AFM-b magnetic state (FM bilayers coupled antiferromagnetically along *c* axis with spin along *b/-b* axis) to G-AFM state which is characterized by the nearest-neighbor AFM coupling for both in-plane and our-of-plane directions.[19-21] For clarity, magnetic phase diagram of Ti doped $Ca_3Ru_2O_7$ systems summarized from previous work is presented in Fig. 2a.[19-21] Samples around the critical composition of phase transition are characterized by a phase separation between the insulating G-AFM phase and weak localized AFM-b phase.[19-21] This phase separation are illustrated by gradient colored and shadowed region in Fig. 2a. The ratio of G-AFM phase to AFM-b phase is very sensitive to the Ti concentration in shadowed region.[21] Electronic ground state evolves from quasi-2D metallic state ($Ca_3Ru_2O_7$) to weak localized state and finally to Mott insulating state. Before the system enters single G-AFM Mott insulating state, it shown complex phase transitions with decreasing temperature. An intermediate magnetic (IM) state emerges between AFM-a and AFM-b/G-AFM. This IM state is consisted by both commensurate and incommensurate magnetic order.[19,20]

2. Experimental procedure

High quality single crystalline samples of $Ca_3(Ru_{0.972}Ti_{0.028})_2O_7$ used in this study were grown by floating zone technique. All samples used for measurements were examined by X-ray diffraction (XRD) and a superconducting quantum interference device (SQUID, Quantum Design) and were shown to be composed of pure bilayered phase. The chemical compositions were determined by Energy-dispersive

X-ray spectroscopy. The in-plane crystallographic directions were determined using Laue X-ray diffraction measurements. Every sample used in the experiments was carefully examined by SQUID to ensure twin-domain free. The magnetoresistivity of the samples were measured with a four-probe method in a physical property measurement system (PPMS, Quantum Design). ρ_{ab} is measured on thin rectangular plate-like samples with size ~ 0.5mm*1mm*0.1mm. Voltage leads are attached on the top surface of the samples. Current Leads are connected to the two opposite side faces of the samples. ρ_c is measured on thin square plate-like samples with size ~ 0.5mm*0.5mm*0.1mm. The current leads are formed by a circular pattern of epoxy with a small notch on the top and bottom of the samples. Voltage leads are attached in the center of the circle. Schematic diagrams of leads configuration are shown in Supplementary material. Both in-plane and out-of-plane resistivity measurements are repeated on several samples. They show consistent magnitude and temperature dependency (see Supplementary material). Samples' dimensions are measured under microscope with precision of 1/45 mm. External magnetic field are applied along in-plane directions *a* or *b*.

3. Results and discussions

The temperature dependent ρ_c/ρ_{ab} for $Ca_3(Ru_{0.972}Ti_{0.028})_2O_7$ is plotted in Fig. 2a. This compound show complex magnetic transitions with temperature. [19,20] It first shows the AFM-*a* order below 65 K, and then evolves into the G-AFM order below T_{MIT} ~ 46 K. Within a very narrow temperature range (40 K – 44 K), the mixed phase is present. There exist three magnetic phases in this mixed phase region: AFM-a, G-AFM and an incommensurate magnetic order (IM). Below 40 K, the incommensurate component vanishes and the weakened AFM-a component transforms into AFM-b with small volume fraction. The G-AFM order survives as a major phase.[19,20]

Let's take a look at the anisotropic ratio at different magnetic phases. In the PM and AFM-a range, ρ_c is one order larger than ρ_{ab} and show weakly temperature dependence. A steep increase of ρ_c/ρ_{ab} on a logarithmic scale to 10^9 happens accompany by the magnetic phase transition from AFM-a to major G-AFM phase. To explore this abnormality, the temperature-dependent in-plane and out-of-plane resistivity within the same temperature range are presented in Fig. 2b inset. Metal-semiconductor/insulator transitions are observed in ρ_{ab} and ρ_c at T_{MIT} respectively. However, ρ_{ab} show semi-conducting/insulating behavior below T_{MIT} with resistivity around only 0.003 Ω cm at 5 K; ρ_c show

insulating behavior with resistivity above 10^6 Ω cm at 5 K. As we state above, layered TMOs can be viewed as self-assembled stacks of two-dimensional materials weakly coupled to each other. Therefore, they always show anisotropic characteristics in charge-transport behavior. However, the anisotropic ratio in $Ca_3(Ru_{0.972}Ti_{0.028})_2O_7$ is 3 orders larger than the largest one observed in perovskite type TMOs. What is the unique mechanism responsible for the huge anisotropic ratio?

To answer this question, we plotted temperature dependent ρ_c/ρ_{ab} for parent compound $Ca_3Ru_2O_7$ (see Fig. 2c) within the same temperature range. In the PM and AFM-*a* range, ρ_c is constantly one order larger than ρ_{ab}, similar to $Ca_3(Ru_{0.972}Ti_{0.028})_2O_7$. A jump of anisotropic ratio happened at T_{MIT} to around 4000. The temperature-dependent in-plane and out-of-plane resistivities within the same temperature range of $Ca_3Ru_2O_7$ are presented in Fig. 2c inset. We found that in-plane resistivity of $Ca_3Ru_2O_7$ are almost at the same order of $Ca_3(Ru_{0.972}Ti_{0.028})_2O_7$ both below and above T_{MIT}. However, out-of-plane resistivity of $Ca_3Ru_2O_7$ are 1 order smaller than $Ca_3(Ru_{0.972}Ti_{0.028})_2O_7$ above T_{MIT}, 9 orders smaller than $Ca_3(Ru_{0.972}Ti_{0.028})_2O_7$ below T_{MIT}. The large bifurcation of anisotropic ratio between $Ca_3(Ru_{0.972}Ti_{0.028})_2O_7$ (~10^9) and $Ca_3Ru_2O_7$ (~ 4000) is caused by the large divergence of ρ_c when the two compounds enter different magnetic phase (G-AFM+AFM-*b* for $Ca_3(Ru_{0.972}Ti_{0.028})_2O_7$ and AFM-*b* for $Ca_3Ru_2O_7$). To clarify the mechanism of huge resistivity anisotropy, the study of magneto-electric coupling is desirable.

Before the study of magneto-electric coupling, I will focus on the magnetic structure first. Isothermal magnetization measurements at typical temperatures (5 K, 10 K and 15 K) for external magnetic field applied along *a* and *b* axis respectively are shown in Fig. 3a and 3b. From our previous study, the $Ca_3(Ru_{0.972}Ti_{0.028})_2O_7$ compound falls in the range of G-AFM and AFM-b coexistence ground state. The volume ratio of these two phases can be estimated from isothermal magnetization measurements. When field is applied along *b* axis, which is the easy axis of both AFM-b and G-AFM phase; *a* first-order metamagnetic transition occurs at ~ 5 T, similar to the metamagnetic transition from AFM-b to canted antiferromagnetic (CAFM) in $Ca_3Ru_2O_7$ whose ground state magnetic structure is solely AFM-b.[22,23] However, the saturated magnetic moment is only around 0.08 μ_B/Ru above the transition field, far away from the expected value of fully polarized spin moment of Ru^{4+} (S = 1, M_s = 2 μ_B/Ru) or the saturated moment of $Ca_3Ru_2O_7$ (~ 1.7 μ_B/Ru). [14,24] There is a trace for the second transition at higher field

since the $M(B)$ curve show a large positive slope above the first transition field (~ 5 T). This result indicates that the volume fraction of AFM-b phase in $Ca_3(Ru_{0.972}Ti_{0.028})_2O_7$ compound is quite low. $M(B)$ for B // a at low temperature (< 30 K) is almost linear as a function of field, up to 7 T (see Fig. 3(c)), indicating no twin domain in this sample.

With temperature increase, the hysteresis of the metamagnetic transition at 5 T is reduced due to the increase of thermal fluctuation, meanwhile, a second transition at higher field appears. This transition is thought to be originated from the polarization of major G-AFM phase based on the evidence below: (1) We extend the isothermal magnetization measurements to temperature range above 30 K (see Fig. 3b), the second transition is completely moved into the equipment capable region (≤ 7 T) and transition field decreases with increasing temperature. The saturated moment for T = 35 K is around 1.5 μ_B/Ru, three quarters of the fully polarized spin moment of Ru^{4+}. It is nature to estimate that at lower temperature, the saturated moment should be more close to 2 μ_B/Ru, with higher transition field, indicating the fully polarization of major phase. (2) When field is applied along a-axis, for temperature above 30 K, the $M(B)$ curve is similar to that for B // b with slightly higher transition field. This is understandable with the approximation above. Due to the canted spin configuration in G-AFM phase: the spin is point to the direction which is ~ 30° to b axis, ~ 60° to a and c axis.[19] Therefore, at same temperature, larger magnetic field is required to polarized spins to a direction.

To study the relationship between transport behavior and magnetic structure, we performed magnetoresistivity measurements. Currents are applied along both in-pane and out-of-plane directions; magnetic fields are along easy axis b. In Fig. 4a, red curve shows the ratio of in-plane resistivity at certain field to that at zero field versus external magnetic field; blue curve exhibits the magnetization of the same sample verses external magnetic field. All data are taken at 10 K. As we state above, the metamagnetic transition at ~ 5 T should have the same origin of the transition in $Ca_3Ru_2O_7$: the spin flip/flop of AFM-b phase, and it only reach a magnetic moment of ~ 0.08 μ_B/Ru. The in-plane magnetoresistivity $\rho_{ab}(B)$ shows a sudden jump right at the metamagnetic transition field (~ 5 T), indicating that the in-plane transport behavior is in strong correlation to the minor AFM-b phase.

How about the interlayer transport behavior? We increase the environment temperature to 35 K to investigate the relationship between $\rho_c(B)$ and the magnetization M. The ratio of interlayer resistivity at

certain field to that at zero field verses magnetic field ($\rho_c(B)/\rho_c(0)$) as well as the magnetization verses magnetic field taken at 35 K are shown in Fig. 4b. Obviously, the huge jump of ρ_c happened at the same field of the polarization of major G-AFM phase. Indicate that the interlayer transport behaviors are closely related to the major G-AFM phase of this material. $\rho_c(B)/\rho_c(0)$ versus magnetic field at 10 K are also plotted as Fig. 4c. Clearly, the sudden jump of ρ_c do not happen at the same field as the metamagnetic transition of AFM-b phase at ~ 5 T. Instead, it happened at a higher field ~ 8 T at 10 K, which corresponds to the polarization field of G-AFM phase even this transition cannot be reflected by magnetization measurements due to equipment limitation.

This highly anisotropic transport behavior is strongly dependent on the magnetic structure. A promising explanation of this feature is in-plane percolation effect. The minor AFM-b phase, even only occupy a small volume fraction, it may form in-plane conducting channel if that AFM-b domains have some sort of internal organizations, such as "stripe shape" domain observed in $Sr_3(Ru_{1-x}Mn_x)_2O_7$.[25] Our-of-plane magnetoresitivity $\rho_c(B)$ should be explained by tunneling magnetoresistance (TMR) effects since that this material is naturally composed of magnetic bilayers (Ru, Ti)O_2 separated by nonmagnetic insulating layers Ca_2O_2. Parallel circuit model can be applied in $\rho_c(B)$. One channel is composed of AFM-b/Ca_2O_2/AFM-b Sandwich structure, resulting a bulk spin valve effect in which ρ_c is very strongly suppressed by the antiferromagnetic alignment. This suppression can be destroyed in favor of ferromagnetism at the critical field of AFM-b polarization (~ 5T). The other channel is composed of G-AFM/Ca_2O_2/G-AFM or G-AFM/Ca_2O_2 /AFM-b layered structure. Considering that AFM-b phase only occupied quite small volume fraction, it is unlikely that the AFM-b ranges overlap at different layers. Field sweep $\rho_c(B)$ measurements confirm this assumption. It shows spin-valve effect at the polarization field of G-AFM phase. The lower resistivity channel which are composed of AFM-b/Ca2O2/AFM-b sandwich structure are turned off. This mechanism can be applied not only in bulk materials, but also in materials that are more commonly used in applications, such as films, hybrid materials and so on. The key point of this new mechanism is to increase the inhomogeneity from one dimensional (along out-of-plane direction) to three dimensional.

4. Conclusions

In summary, we observed highly anisotropic transport properties for currents applied along and perpendicular to *c*-axis in $Ca_3(Ru_{0.972}Ti_{0.028})_2O_7$ compound. The change of magnetoresistivity in a magnitude ~ 50% and ~ 10^8 are obtained for ρ_{ab} and ρ_c respectively for field along *b*-axis. This unique magneto-electronic coupling is possibly attributed to the electronic phase separated ground state and in-plane percolation effect. This special case may stimulate a new path for reducing current leakage and power consumption in electronic devices.

Acknowledgements

This work is supported by the Natural Science Foundation of China (Nos. 11304149, U1332205, 11274153, 11204124, 51202108).The work at Tulane is supported by the U.S. Department of Energy under EPSCoR Grant No. DE-SC0012432 with additional support from the Louisiana Board of Regents (support for crystal growth and magnetic measurements) and NSF under Grant DMR-1205469. J. P. conducted crystal growth, structural characterization, magnetization and transport measurements; wrote the manuscript. X. G., G. Z. and W. W. contributed to transport measurements in part. J. L. and J. H. contributed to magnetization measurements in part. X. S. Wu supervised the project. All authors reviewed and commented on the manuscript. We are also thankful to a number of researchers who critically commented on an earlier version of this manuscript or provided helpful input: Z. Q. Mao (Tulane University), Mingqiang Gu (Northwesten University) and Yuechun Shi (Nanjing University).

References

[1] E. Dagotto, Science **309**, 257 (2005).
[2] K. A. M. J. G. Bednorz, Zeitschrift fur Physik B Condensed Matter **64**, 189 (1986).
[3] A. P. Ramirez, Journal of Physics: Condensed Matter **9**, 8171 (1997).
[4] S. N. Ruddlesden and P. Popper, Acta Crystallographica **10**, 538 (1957).
[5] S. N. Ruddlesden and P. Popper, Acta Crystallographica **11**, 54 (1958).
[6] A. M. Haghiri-Gosnet and J. P. Renard, Journal of Physics D: Applied Physics **36**, R127 (2003).
[7] J. Heremans, Journal of Physics D: Applied Physics **26**, 1149 (1993).
[8] S. Fujii, Y. Suzuki, J. Kawamata, and R. Tsunashima, Journal of Materials Chemistry C **3**, 7153 (2015).
[9] A. M. Nardes, M. Kemerink, R. A. J. Janssen, J. A. M. Bastiaansen, N. M. M. Kiggen, B. M. W. Langeveld, A. J. J. M. van Breemen, and M. M. de Kok, Adv Mater **19**, 1196 (2007).
[10] S. Ono and Y. Ando, Phys Rev B **67**, 104512 (2003).
[11] T. G. Perring, G. Aeppli, T. Kimura, Y. Tokura, and M. A. Adams, Phys Rev B **58**, R14693 (1998).
[12] J. F. Hulvat and S. I. Stupp, Adv Mater **16**, 589 (2004).
[13] Q. Wei, M. Mukaida, K. Kirihara, and T. Ishida, ACS Macro Letters **3**, 948 (2014).
[14] G. Cao, S. McCall, J. E. Crow, and R. P. Guertin, Phys Rev Lett **78**, 1751 (1997).
[15] Y. Yoshida, I. Nagai, S.-I. Ikeda, N. Shirakawa, M. Kosaka, and N. Môri, Phys Rev B **69**, 220411 (2004).
[16] J. S. Lee, S. J. Moon, B. J. Yang, J. Yu, U. Schade, Y. Yoshida, S. I. Ikeda, and T. W. Noh, Phys Rev Lett **98**, 097403 (2007).
[17] H. L. Liu, S. Yoon, S. L. Cooper, G. Cao, and J. E. Crow, Phys Rev B **60**, R6980 (1999).
[18] F. Baumberger *et al.*, Phys Rev Lett **96**, 107601 (2006).
[19] X. Ke, J. Peng, D. J. Singh, T. Hong, W. Tian, C. R. Dela Cruz, and Z. Q. Mao, Phys Rev B **84**, 201102 (2011).
[20] J. Peng, X. Ke, G. Wang, J. E. Ortmann, D. Fobes, T. Hong, W. Tian, X. Wu, and Z. Q. Mao, Phys Rev B **87**, 085125 (2013).
[21] J. Peng, J. Y. Liu, J. Hu, Z. Q. Mao, F. M. Zhang, and X. S. Wu, Scientific Reports **6**, 19462 (2016).
[22] W. Bao, Z. Q. Mao, Z. Qu, and J. W. Lynn, Phys Rev Lett **100**, 247203 (2008).
[23] Y. Yoshida, S.-I. Ikeda, H. Matsuhata, N. Shirakawa, C. H. Lee, and S. Katano, Phys Rev B **72**, 054412 (2005).
[24] Z. Qu *et al.*, Phys Rev B **78**, 180407 (2008).
[25] M. A. Tae-Hwan Kim, B. Hu, R. Jin, X.-G. Zhang, J. F. Wendelken, E. W. Plummer, and An-Ping Li, PNAS **107**, 5272 (2010).

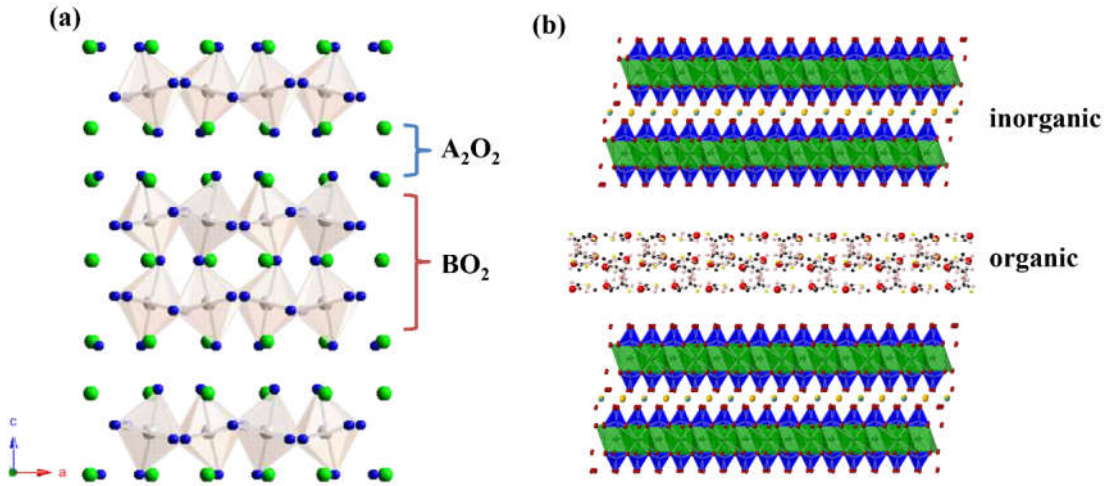

Figure 1: Schematic diagrams of crystal structures of (a) RP type layered materials $A_{n+1}B_nO_{3n+1}$ (n = 2); (b) organic-inorganic hybrids materials. Lower conductivity A_2O_2 (a) or inorganic (b) layers and higher conductivity BO_2 (a) or organic (b) layers are labeled in the diagrams.

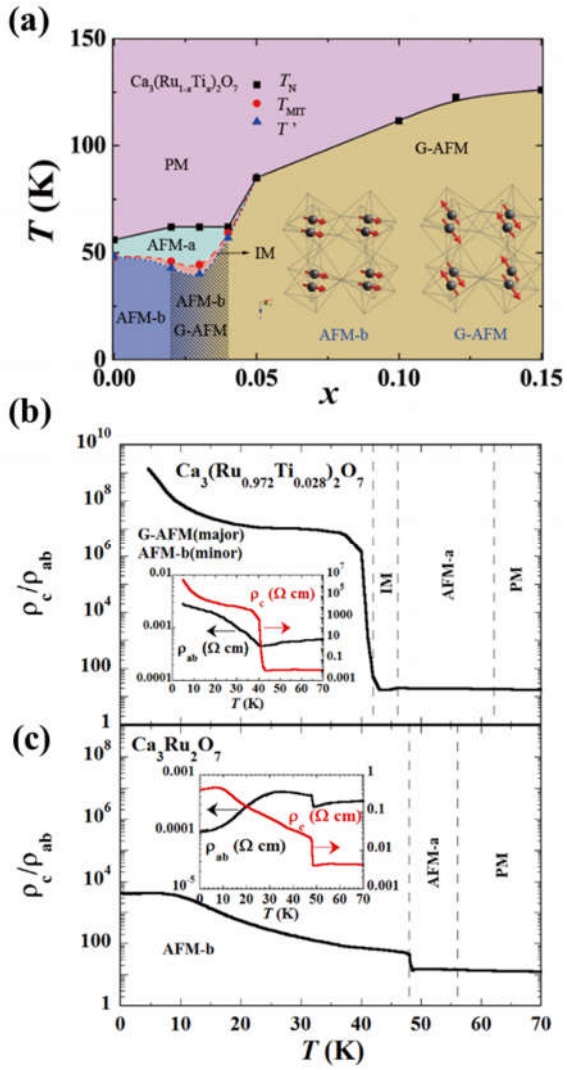

Figure 2: (a) Magnetic phase diagram of $Ca_3(Ru_{1-x}Ti_x)_2O_7$ ($0 \leqslant x \leqslant 0.15$). Distinct magnetic phases are represented by different colors and labels. Magnetic phase separation regions are illustrated by a shadow with gradient color background. Inset: Schematic diagrams of AFM-b and G-AFM magnetic structures. (b) Temperature dependence of ρ_c/ρ_{ab} of $Ca_3(Ru_{0.972}Ti_{0.028})_2O_7$. PM: paramagnetic; IM: incommensurate magnetic phase; G-AFM: G-type antiferromagnetic. Inset: temperature dependence of the in-plane (ρ_{ab}) and out-of-plane (ρ_c) resistivity for $Ca_3(Ru_{0.972}Ti_{0.028})_2O_7$. (c) Temperature dependence of ρ_c/ρ_{ab} of $Ca_3Ru_2O_7$. Inset: temperature dependence of the in-plane (ρ_{ab}) and out-of-plane (ρ_c) resistivity for $Ca_3Ru_2O_7$.

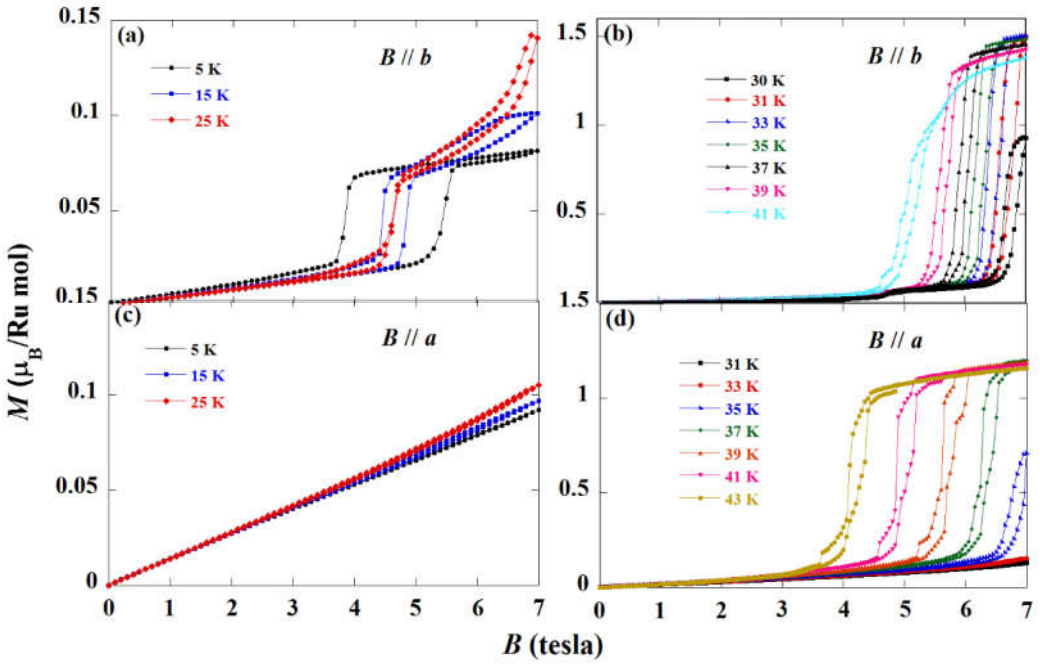

Figure 3: Magnetization versus external magnetic field at different temperature: (a) Magnetization for *B // b* measured at 5 K, 15 K and 25 K respectively. (b) Magnetization for *B // b* measured at 30 K, 31 K, 33 K, 35 K, 37 K, 39 K and 41 K respectively. (c) Magnetization for *B // a* measured at 5 K, 15 K and 25 K respectively. (d) Magnetization for *B // a* measured at 31 K, 33 K, 35 K, 37 K, 39 K, 41 K and 43 K respectively.

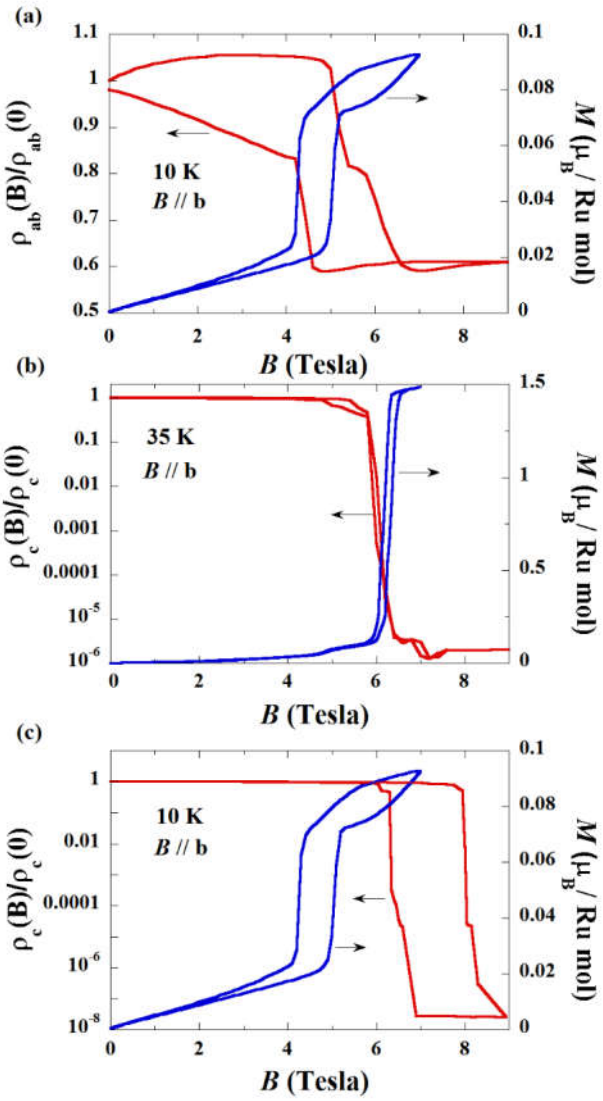

Figure 4: (a) Magnetic field dependent in-plane resistivity (ρ_{ab}) and magnetization taken at 10 K with field applied along *b*-axis. (b) Magnetic field dependent out-of-plane resistivity (ρ_c) and magnetization taken at 35 K with field applied along *b*-axis. (c) Magnetic field dependent out-of-plane resistivity (ρ_c) and magnetization taken at 10 K with field applied along *b*-axis.